A Comparison of Large Eddy Simulations of Wind and Ocean Turbines

Ryan King and Spencer Alexander

December 13th, 2012

1 Introduction

High fidelity modeling of fluid flow is crucial in calculating mechanical loads, power production, and wake behaviors of wind and ocean turbines. The wind industry has suffered from unexpected gearbox failures and underperformance, and recent publications attribute these effects to poor characterization and prediction of the turbulent flow fields experienced by wind turbines. To alleviate these effects, CFD calculations must be able to model realistic atmospheric and ocean boundary layers flows that occur in wind and ocean turbine installations. In particular, these CFD simulations must account for turbulent coherent structures that are the primary cause of fatigue damage to wind turbine blades and drivetrains [9, 10]. Additionally, these CFD simulations must include thermal stability effects because stability has been shown to impact the power production of single turbines and affect the wake behavior from arrays of turbines [18, 17]. More accurate modeling of these turbulent flow fields will lead to improved wind turbine reliability and more energetic wind farm arrays, ultimately lowering the cost of renewable energy.

In response to these concerns, there have been several new developments in computational modeling of wind farms. In particular, large eddy simulations (LES) have been used to model wind turbines and their arrays in realistic atmospheric boundary layer (ABL) flows [4, 11, 13, 19, 14]. Additionally, recent work models arrays of tidal-current turbines [7] in a shallow channel. In this study we take an LES approach to generating realistic neutrally stable and convective ABL's, and extend that framework to a stable ocean boundary layer (OBL). This approach builds on the Simulator for Offshore Wind Farm Applications (SOWFA) toolset developed by Matt Churchfield and Sang Lee at the National Wind Technology Center [2]. This toolset uses OpenFOAM, an open source finite volume CFD program [1], to generate precursor boundary layer simulations exhibiting realistic turbulent structures. Actuator line models of wind and ocean turbines are then inserted into the fully developed boundary layer flows following the work of Churchfield and Troldborg [6, 5, 16]. Our results show interesting differences in the wake behaviors of ocean and atmospheric turbines that have important implications for array optimization. Additionally, we discuss the emergence of numerical artifacts and comment on their impact on the choice of LES grid cell size.

2 Methodology

2.1 Physics

LES

In this study, we employ a Large Eddy Simulation (LES) to model the fluid flow in the atmospheric and ocean boundary layers. In an LES simulation a low pass spatial filter is applied to the incompressible Navier-Stokes equations so that the scales of turbulence responsible for transport and production of turbulent kinetic energy (TKE) are directly resolved, but smaller scales where viscous dissipation takes place are parameterized in a sub-filter scale model (SFS) [12]. The governing equations for our simulation include the Boussinesq approximation for buoyancy effects, Coriolis forces for a latitude of 45 deg north, driving pressure force, temperature gradient force, and density-normalized forces representing our turbine actuator model. The governing equations are the filtered continuity equation,

$$\frac{\partial \bar{u}_j}{\partial x_j} = 0, \tag{1}$$

the filtered momentum equation,

$$\frac{\partial \bar{u}_i}{\partial t} + \frac{\partial}{\partial x_j}\left(\bar{u}_j \bar{u}_i\right) = -2\varepsilon_{i3k}\Omega_3 \bar{u}_k - \frac{\partial \tilde{p}}{\partial x_i} - \frac{1}{\rho_0}\frac{\partial p_0}{\partial x_i} - \frac{\partial \tau_{ij}^D}{\partial x_j} + g\left(\frac{\bar{\theta} - \theta_0}{\theta_0}\right) + \frac{1}{\rho_0}F_i^T \tag{2}$$

where

$$\tilde{p} = \frac{\bar{p} + \tau_{kk}}{3\rho}, \tag{3}$$

and the potential temperature transport equation

$$\frac{\partial \bar{\Theta}}{\partial t} + \frac{\partial}{\partial x_j}\left(\bar{u}_j \bar{\Theta}\right) = -\frac{\partial}{\partial x_j}\left(q_j\right) \tag{4}$$

The SFS model is used to parameterize viscous effects and is the standard Smagorinsky model. This SFS model accounts for shear stress everywhere except at the lower boundary where a wall model is used. The SFS model is applied at cell faces, which avoids interpolating to cell faces while taking the divergence of stress but provides a less dissipative effect near the lower boundary surface. To model this, the shear stress equation is set to

$$\tau_{ij}^D = -2\nu^{SFS}\bar{S}_{ij}, \tag{5}$$

where

$$\bar{S}_{ij} = \frac{1}{2}\left(\frac{\partial \bar{u}_i}{\partial x_j} + \frac{\partial \bar{u}_j}{\partial x_i}\right). \tag{6}$$

The Smagorinsky model defines ν as

$$\nu^{SFS} = (C_s\Delta)^2(2\bar{S}_{ij}\bar{S}_{ij})^{1/2} \tag{7}$$

where C_s is the model constant set to 0.125 and Δ is the filter length scale, which for SOWFA is set as $(\Delta x \Delta y \Delta z)^{1/3}$.

Because of the sharp velocity gradients, complex surface roughness effects, and vortical structures that exist near the lower wall boundary, a wall model is applied at the lower boundary instead of directly resolving the flow with a no-slip condition. This wall model accounts for the momentum and heat flux at the wall. In this study we apply Moeng's wall model, which estimates a friction velocity based on supplied roughness heights and surface temperature flux using the Monin-Obukhov similarity theory [12]. This friction velocity then leads to the horizontally averaged shear stresses on the lower surface. The relevant equations for surface shear stress are,

$$\tau_{ij}^{D} = \begin{bmatrix} 0 & 0 & \tau_{13}^{tot} \\ 0 & 0 & \tau_{23}^{tot} \\ \tau_{13}^{tot} & \tau_{23}^{tot} & 0 \end{bmatrix}. \tag{8}$$

τ_{13}^{tot} and τ_{23}^{tot} are defined as,

$$\tau_{13}^{tot} = -u_*^2 \frac{S_{1/2}\langle \bar{u}_{1/2} \rangle + \langle S_{1/2} \rangle \left(\bar{u}_{1/2} - \langle \bar{u}_{1/2} \rangle \right)}{\langle S_{1/2} \rangle \left(\langle \bar{u}_{1/2} \rangle^2 + \langle \bar{v}_{1/2} \rangle^2 \right)^{1/2}}, \tag{9}$$

$$\tau_{23}^{tot} = -u_*^2 \frac{S_{1/2}\langle \bar{v}_{1/2} \rangle + \langle S_{1/2} \rangle \left(\bar{v}_{1/2} - \langle \bar{v}_{1/2} \rangle \right)}{\langle S_{1/2} \rangle \left(\langle \bar{u}_{1/2} \rangle^2 + \langle \bar{v}_{1/2} \rangle^2 \right)^{1/2}}, \tag{10}$$

where u_*^2 is the friction velocity, which can be calculated from the Obukhov length and aerodynamic roughness length.

Turbine Properties

The turbines modeled in our two simulation were not modeled as physical blades to which the fluid provided with rotational energy – the computation power and modeling difficulty of such blades are beyond the scope of this paper. Instead, the turbines were modeled as a set of actuator lines which impose body forces on the incoming fluid flow. This model is described by Sorensen and Shen [15] and implimented in SOWFA [2].

For the onshore wind turbine simulations we used the NREL Offshore 5-MW Baseline Wind Turbine [8], which is a representative utility scale multi-megawatt wind turbine developed at NREL's National Wind Technology Center. It is based on the REpower 5M wind turbine, with additional data from other publicly available sources so that the structural, aerodynamic, material, and control system properties are representative of a modern day wind turbine. The wind turbine is three-bladed, upwind, variable speed, pitch controlled turbine with a 126 m rotor diameter, 90 m hub height, and high speed multi-stage gearbox. Rated power for the turbine is 5.0 MW at 12.1 rpm. Mass, stiffness, damping, and airfoil properties are given in NREL documentation [8].

For the ocean current turbine simulation, a 1MW turbine was modeled (hereafter referred to as the OT1MW), with specs based upon the Voith 1 MW [3]. The OT1MW was modeled with a 8 meter blade radius and 1.5m hub. The airfoils used on the OT1MW were a scaled down version of the airfoils used on the NREL5MW turbine as found in the SOWFA package

[2], which is a poor approximation to the Voith 1MW turbine; future work will include a better representation of the 1MW turbine blade and generator properties. The OT1MW produced as expected, with the turbine reaching a steady state production of 0.85MW and steady rotation rate of 8 RPM at hub-height channel velocity of 1.9 m/s.

2.2 Numerics

The numerical package used in the simulations was OpenFOAM (Open Source Field Operation and Manipulation), which is a collection of C++ libraries for solving PDE's on unstructured meshes using the finite volume method [1]. OpenFOAM is increasingly becoming the CFD package of choice for wind turbine simulations thanks to it's open source and adaptable nature that has led to work done at the National Wind Technology Center, the University of Massachusetts Amherst and elsewhere.

We employ the ABLPisoSolver developed as part of the NREL SOWFA (Simulator for Offshore Wind Farm Applications) tool set [2] to solve our flow simulations. ABLPisoSolver is based on the standard PISO algorithm that solves the momentum equation implicitly with the buoyancy, SFS stress, and Coriolis terms. With this solution for $\bar{u}$, the laplacian equation for the pressure field is solved, the momentum flux is calculated from the pressure field, and pressure and momentum flux are corrected iteratively such that the continuity equation is satisfied. In our precursor runs, 2-4 iterations of the pressure field was sufficient to ensure continuity.

2.3 Simulation

Mesh

The atmospheric boundary layer precursor simulation was performed on a domain of 3000 m in the x-direction, 3000 m in the y-direction, and 1000 m in the z direction. The mesh for the precursor simulation was composed of 75x75x25 grid cells, giving a 40m resolution in each direction. The mesh was then decomposed into 6 smaller domains for parallel processing in MPI (Message Passing Interface) using a Scotch decomposition method. Finally, each decomposed domain was refined by a factor of two in all three coordinate directions, increasing the total number of cells eightfold to 1125000. Additionally, the grid was refined three times around the actuator, giving a resolution of 2.5m near the wind turbine and 0.2 meters near the ocean turbine. As discussed later, this grid refinement leads to artifacts in the results.

For the ocean current turbine simulation, the precursor domain size was 200 meters in the x-direction, 200 meters in the y-direction and 70 meters in the z-direction. The initial mesh in the precursor was set at 45x45x20 and was refined once. Each cell in the precursor measured approximately 2x2x1.5 meters.

For both the ocean and ABL simulations, the grid resolutions used in the precursor stage were much coarser than the grid resolutions in our actuator line simulations. While the grid resolution for actuator line was sufficient for accurate results, the resolution of the precursor will need to be increased substantially to ensure realistic inflow conditions. Future work will

study the impact of domain cell resolution in the precursor step and it's impact on both realistic inflow and agreement with the actuator line simulations.

Flow Conditions

To generate realistic turbulent structures, we took the approach of running a precursor simulation that allowed atmospheric or ocean boundary layers to fully develop. Once the boundary layer was fully developed, we then inserted actuator line turbines into the simulation. The initial conditions for our simulations were a uniform velocity from 225° at 1.9 m/s and 9 m/s for ocean and wind, with perturbations added near the surface to cause the turbulent flow field to quickly develop. The solver properties were specified such that the velocity at hub height would be 1.9 m/s and 9 m/s for ocean and wind, and the driving pressure gradient was adjusted to maintain that velocity. The aerodynamic surface roughness in both cases z_0 was 0.016 meters. For the ABL, the temperature profile was constant at 300 K up to 750 m height where the temperature then increased to 308 K. This creates a capping inversion that defines the boundary layer and slows the vertical growth of the boundary layer that has been a problem in previous simulations. The ocean simulation used a constant temperature of 300 K. Surface temperature flux was set to 0 in the neutral ABL case and 0.04 mK/s in the unstable ABL case.

The boundary conditions during the precursor simulation on the top of the domain were: temperature gradient equal to that of the initial capping inversion, normal velocity and parallel velocity gradient equal to zero, the normal pressure gradient from the momentum equation, and zero gradient of SFS viscosity. On the bottom: prescribed temp flux, the normal pressure gradient from momentum equation, and normal velocity equal to zero, horizontal velocity from wall model (nonzero because OpenFOAM is a collocated code). Lateral walls used periodic boundary conditions to generate turbulent structures, and small perturbations were introduced on the bottom of the domain to accelerate their development.

The fully developed precursor simulation was run for an additional 2000 seconds, and slices of inflow data were saved at 0.5 second intervals to be used as boundary conditions in the actuator simulations.

3 Results

3.1 Precursor Results

After 12000 seconds of simulation time, the ABL precursor simulation showed fully developed atmospheric boundary layers. This was ample time to develop the realistic coherent turbulent structures that are crucial to generating realistic loading conditions. The temperature profile of the precursor ABL simulation shows the capping inversion that limits boundary layer growth and vertical motion above 750 m. Figures 1 and 2 show the fully developed flow fields for neutral and unstable ABL's after they've been allowed to spin up for 12000 seconds. As expected, the unstable case shows greater mixing in the boundary layer, while the stable case shows more horizontal velocity shear.

The OBL Precursor was run to 6000 seconds, which represents seven large-eddy turnovers [6]. At this point, the pressure gradient drove our velocity at 35 meters to 1.9 m/s and 2.2

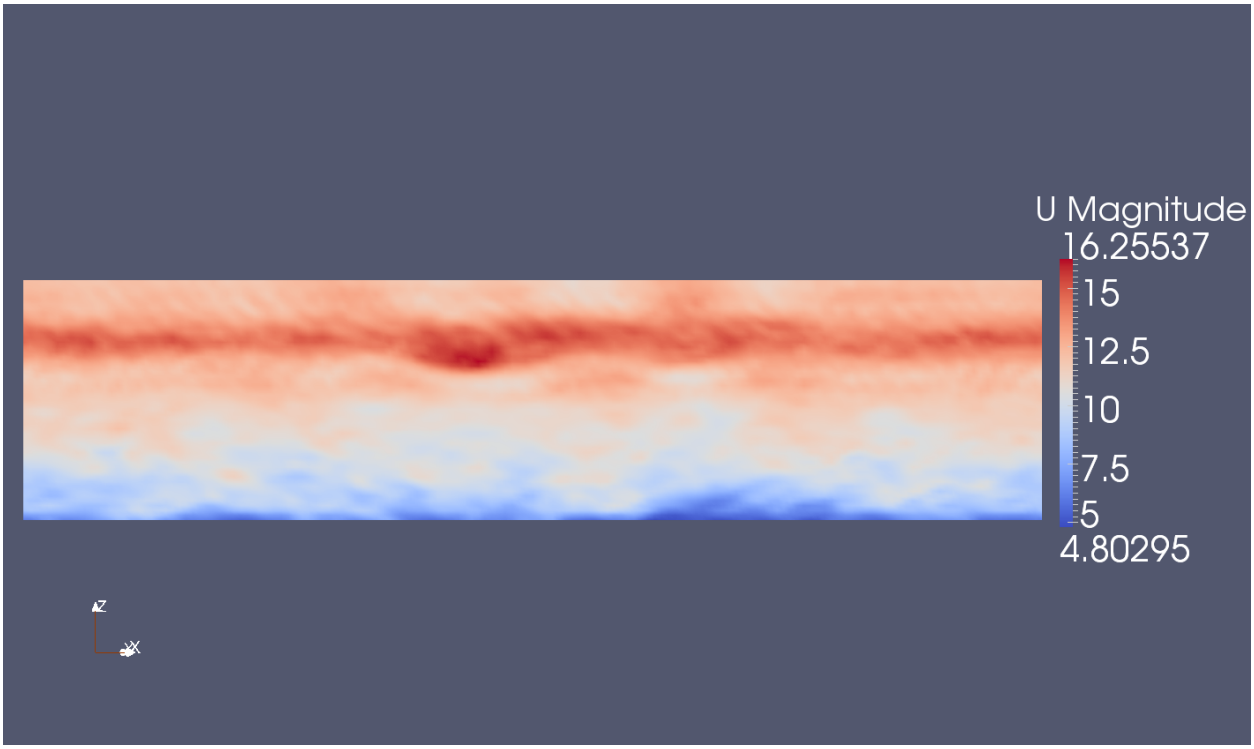

Figure 1: Precursor flow for the neutral ABL case

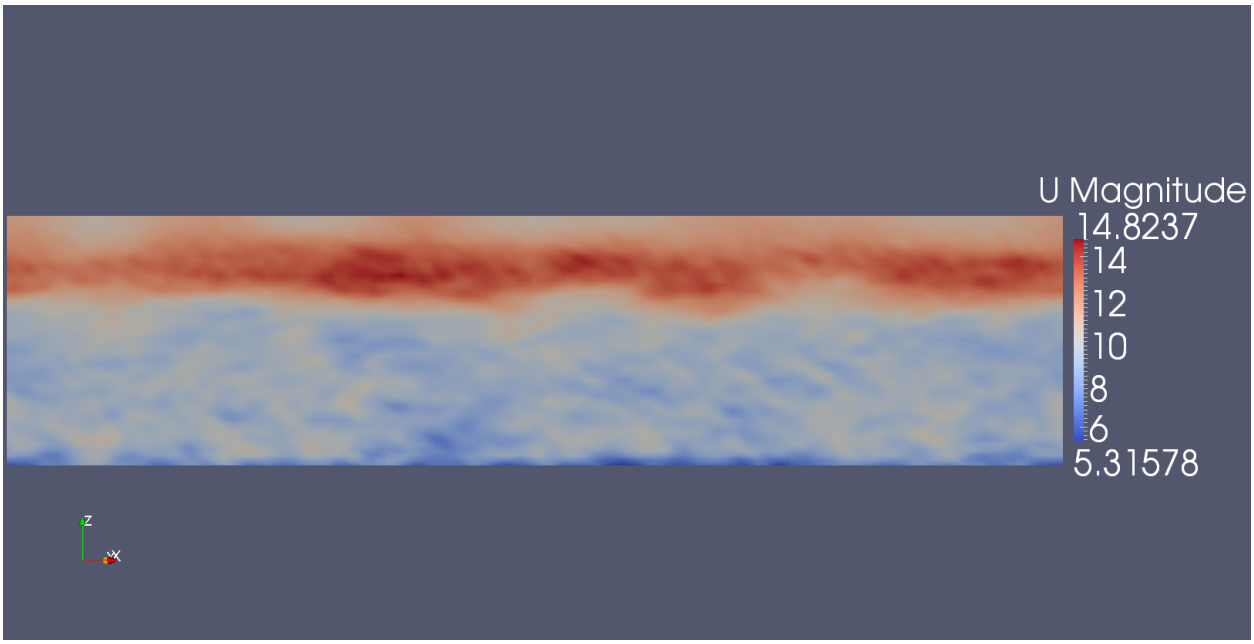

Figure 2: Precursor flow for the unstable ABL case

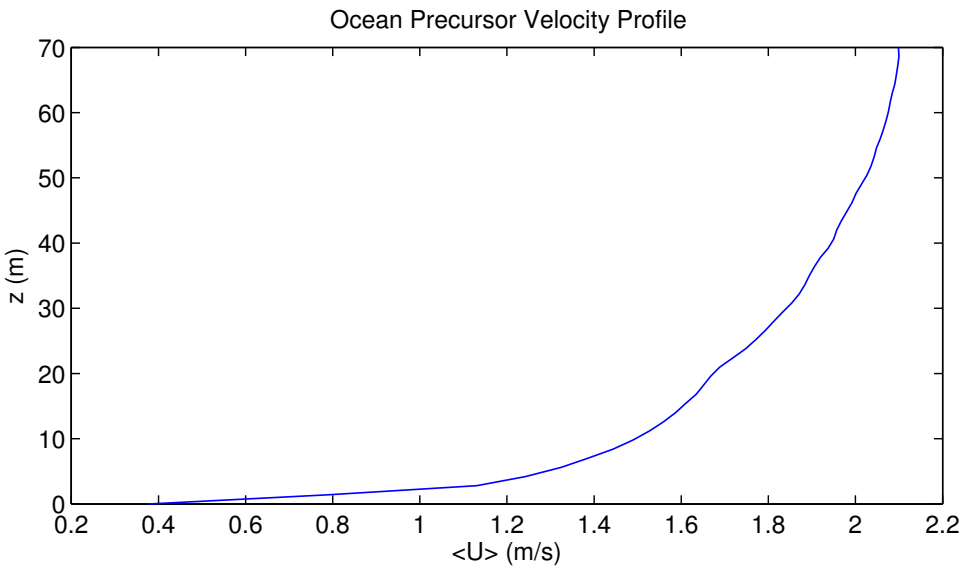

Figure 3: Vertical profile of horizontal velocity for the OBL

m/s. The vertical velocity profile for the flow is shown in Figure 3. Only the stable case was run for the ocean.

3.2 Actuator Line Results

After fully developing the boundary layers in the absence of wind turbines, we insert a single actuator line turbine and run the simulation for another 250-300 seconds. The results lead to several interesting insights. First, there is nontrivial flow leakage at the root of the blades that persists for about two rotor diameters downstream. This region where the blade airfoil properties are still discernible is the "near-wake" region [14]. Further downstream in the "far-wake" region the blade-specific effects have diffused into an amorphous wake, but the velocity deficit that is characteristic of the far-wake is present for eight to ten rotor diameters. Figures 4 and 5 show average velocity profiles at hub height and Figures 6 and 7 show instantaneous velocity profiles after 250 seconds. The instantaneous ABL wake deficits show some wander, but significantly less than will be seen in the ocean turbine wake.

Numerical Artifacts

We observe numerical artifacts in the CFD results located at the transition between grid refinement regions. Figure 8 shows the average velocity at hub height for the unstable ABL with the actual grid cells overlaid on the flow field. Clearly, the artifacts are generated at the abrupt transition between adjacent refinement levels. Confirming these results, the ocean turbine simulation, where the grid refinement was constant across the entire domain, did not show any signs of artifacts – this is shown in Figure 9. However, a single grid refinement level is not the ideal solution – conversations with the SOWFA creators, Matt Churchfield and Sang Lee, suggest that a spatial filter or mesh smoothing function could help alleviate these anomalies.

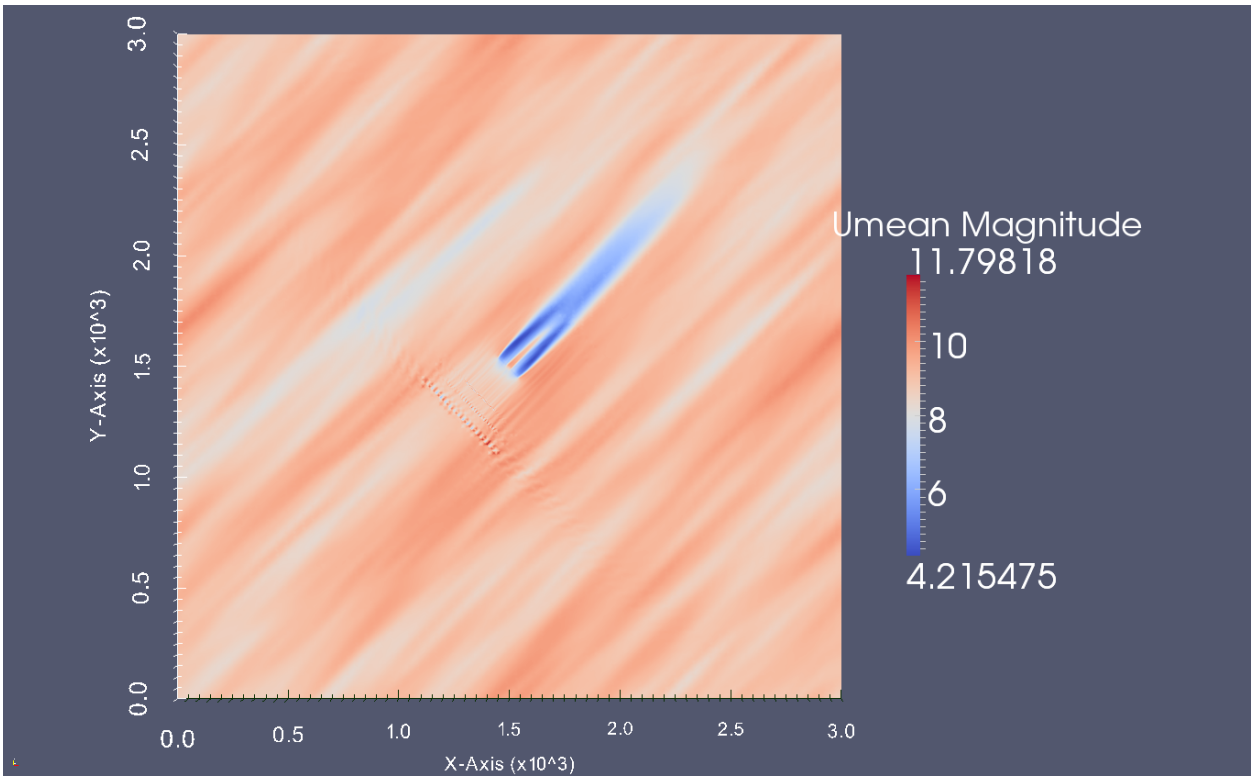

Figure 4: Average hub-height velocity over 250 seconds for the neutral ABL

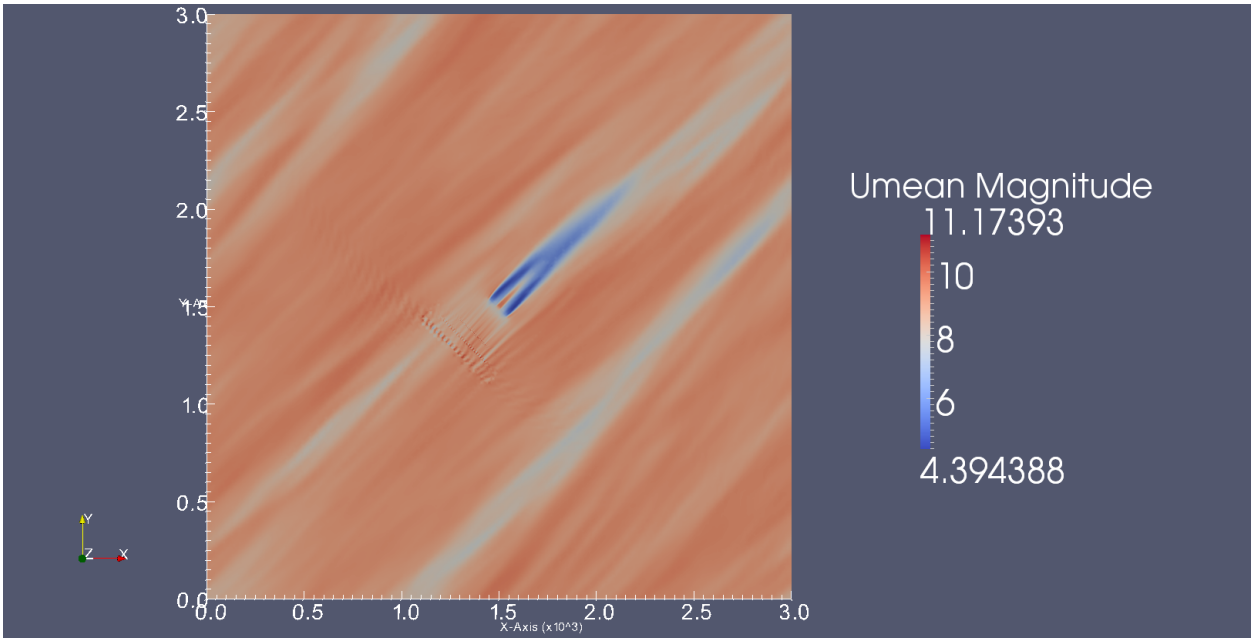

Figure 5: Average hub-height velocity over 250 seconds for the unstable ABL

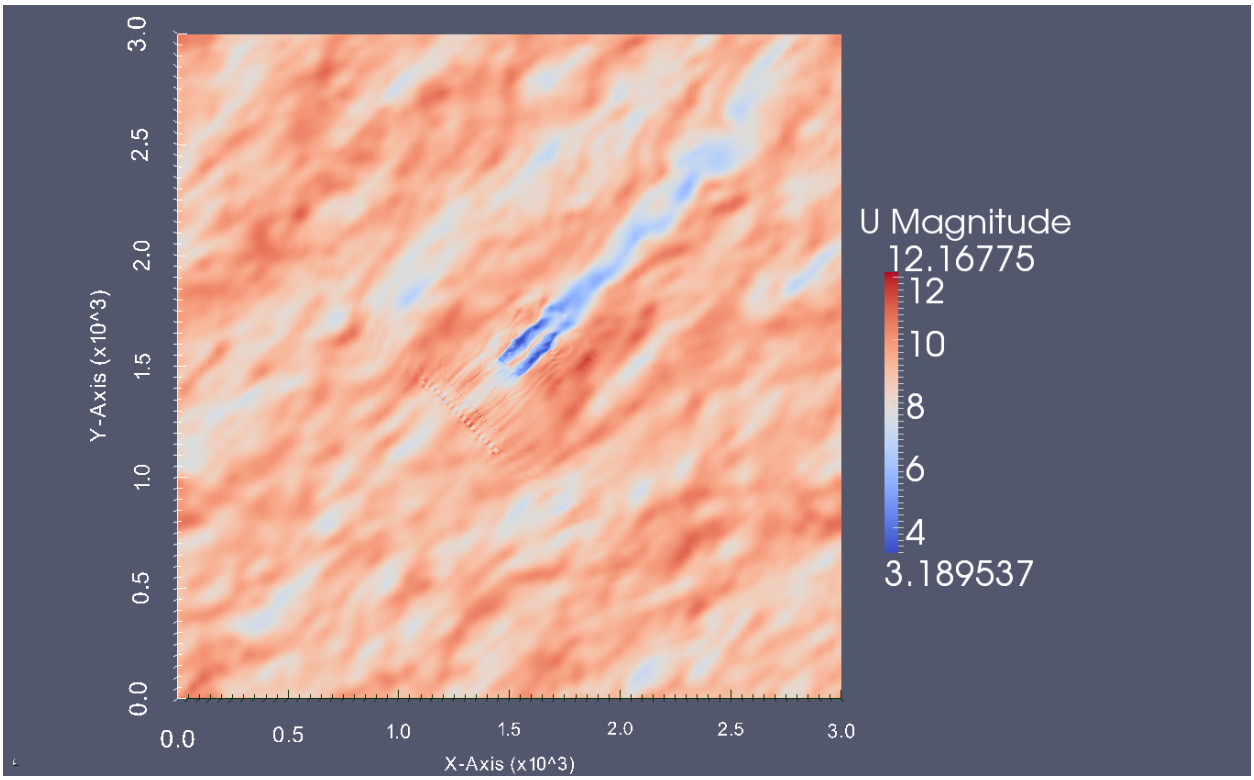

Figure 6: Instantaneous hub-height velocity after 250 seconds for the neutral ABL

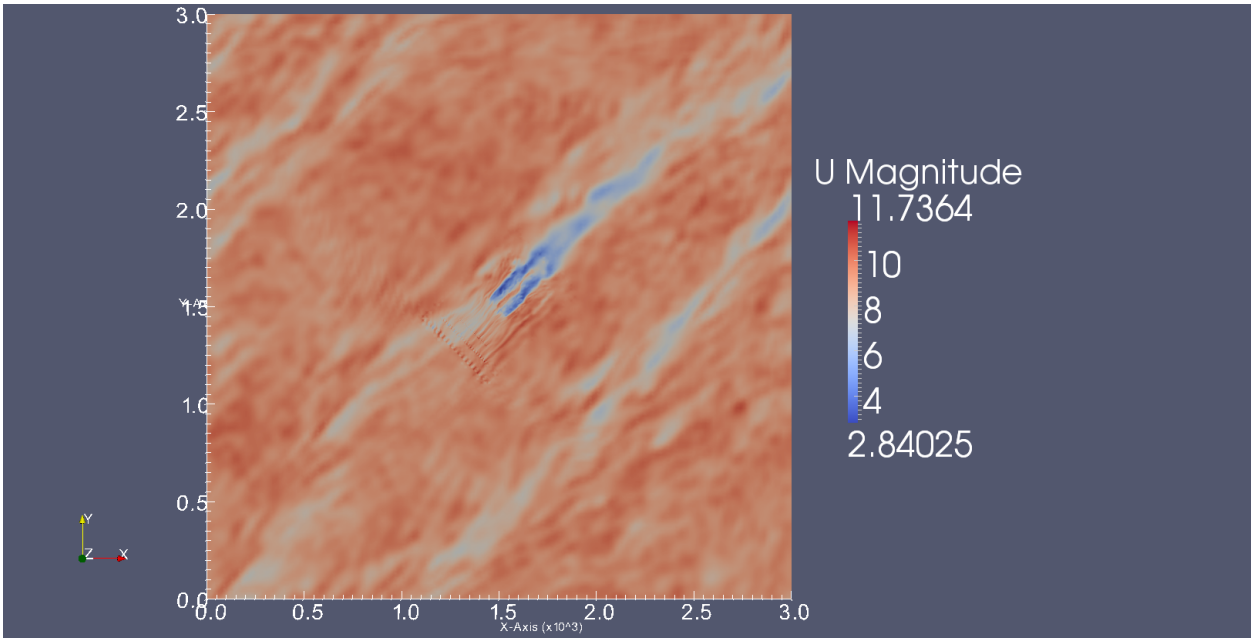

Figure 7: Instantaneous hub-height velocity after 250 seconds for the unstable ABL

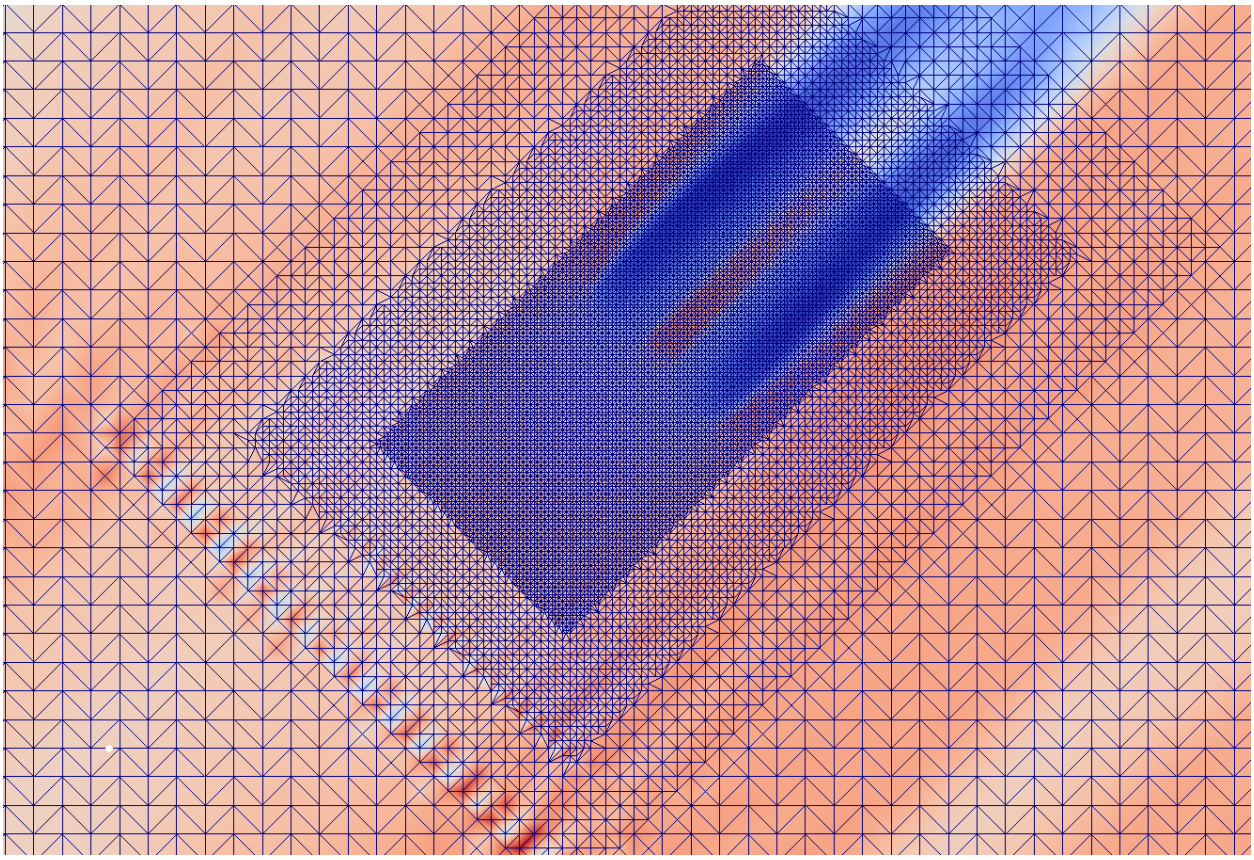

Figure 8: Numerical artifacts present in the ABL wind turbine simulation

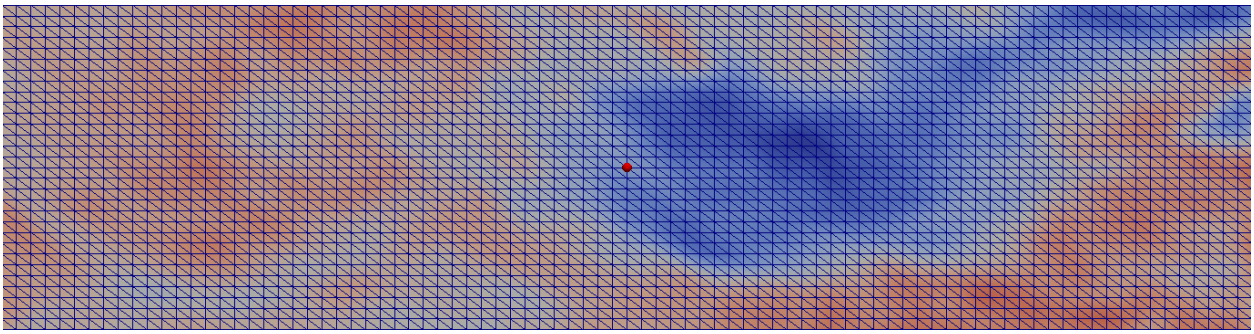

Figure 9: Ocean wind turbine simulation without artifacts

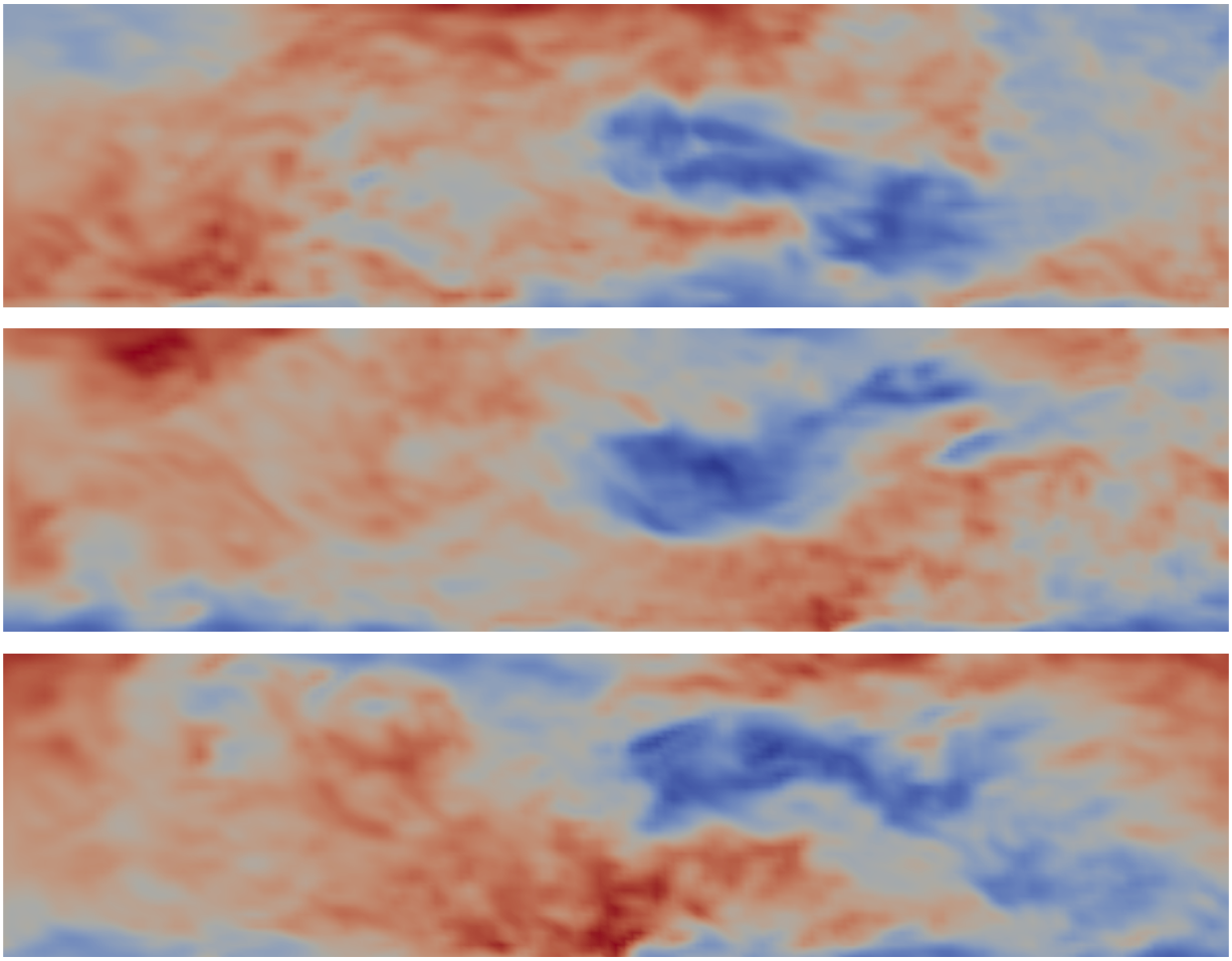

Figure 10: Ocean turbine flow snapshots at t = 100s, 200s and 300s

Vertical wake oscillation

One very notable feature of the ocean current turbine flow was the extent to which vertical flow oscillation dominated the velocity profile. Figure 10 shows the movement of the vertical oscillation, with three snapshots from 100, 200 and 300 seconds. While vertical oscillations were certainly noted in the wind energy simulation, the extent of the ocean turbine oscillation is comparatively much greater, with the peaks of the oscillation covering most all of the 70 meter vertical domain.

4 Conclusion and Future Work

This study replicated existing work on LES simulations of wind turbines, and confirmed many previous findings. Specifically, our ABL simulations showed the wakes dissipating sooner in the unstable case, which fits with other published findings. We also replicated anomalous results due to grid refinement that was originally observed by the creators of the SOWFA tool set. We have extended the SOWFA tool set to ocean boundary layers and

demonstrated much greater periodic motion of the wake in the vertical direction for this shallow ocean flow simulation. Our ocean simulation also shows that the artifacts disappear when grid resolution step changes are removed.

There is a clear need for future work on LES modeling of wind turbines, and we believe there are many opportunities to improve the numerical methods deployed in SOWFA. With the simplicity of the domain, the tendency towards smooth functions and the periodic boundary condition, spectral methods and wavelet decompositions would likely result in a substantial performance gain. Additionally, our simulations used the backward Euler method for time steps, where a performance would likely be gained in using the Crank Nicholson or Runge Kutta methods.

Future work on atmospheric turbine modeling will likely focus on including aero-elastic tools such as the NWTC's FAST aero-elastic simulator, as well as expanding the actuator line tools to larger turbine arrays in more complicated terrain. SOWFA's modular nature will allow for detailed mechanical loads analysis of a single turbine, or broader resource assessment and turbine layout optimization.

Future work on this project related to ocean turbine modeling includes several possibilities. For one, the grid size used in the initial model was very coarse, with a grid cell size of $2m^3$ in the precursor stage and $0.2m^3$ in the turbine modeling stage. A more accurate representation of the precursor flow could be obtained by doubling or tripping the resolution. Second, work remains on better modeling the various tidal turbines currently being proposed by the private sector; the model used in this paper was adapted from a wind turbine design. And finally, work remains in modeling various ocean states, such as stable, unstable, high wind shear/turbulence, etc.

References

[1] Openfoam - the open source computational fluid dynamics (cfd) toolbox, Dec. 2012.

[2] Sowfa - simulator for offshore wind farm applications, Dec. 2012.

[3] Voith - tidal current power stations, Dec. 2012.

[4] M. Calaf, C. Meneveau, and J. Meyers. Large eddy simulation study of fully developed wind-turbine array boundary layers. *Physics of Fluids*, 22:015110–015110–16, Jan. 2010.

[5] M. J. Churchfield, S. Lee, J. Michalakes, and P. J. Moriarty. A numerical study of the effects of atmospheric and wake turbulence on wind turbine dynamics. *Journal of Turbulence*, page N14, 2012.

[6] M. J. Churchfield, S. Lee, P. J. Moriarty, L. A. Martinez, S. Leonardi, G. Vijayakumar, and J. G. Brasseur. A large-eddy simulation of wind-plant aerodynamics: Preprint. Jan. 2012.

[7] M. J. Churchfield, Y. Li, and P. J. Moriarty. Large-eddy simulation study of wake propagation and power production in an array of tidal-current turbines: Preprint. July 2011.

[8] J. Jonkman, S. Butterfield, W. Musial, and G. Scott. Definition of a 5-MW reference wind turbine for offshore system development. Technical report, Feb. 2009.

[9] N. D. Kelley, B. J. Jonkman, G. N. Scott, J. T. Bialasiewicz, and L. S. Redmond. Impact of coherent turbulence on wind turbine aeroelastic response and its simulation: Preprint. Aug. 2005.

[10] S. Lee, M. Churchfield, P. Moriarty, J. Jonkman, and J. Michalakes. Atmospheric and wake turbulence impacts on wind turbine fatigue loading: Preprint. Dec. 2011.

[11] H. Lu and F. PortÃ©-Agel. Large-eddy simulation of a very large wind farm in a stable atmospheric boundary layer. *Physics of Fluids*, 23(6):065101, 2011.

[12] C.-H. Moeng. A large-eddy-simulation model for the study of planetary boundary-layer turbulence. *Journal of the Atmospheric Sciences*, 41(13):2052–2062, July 1984.

[13] F. PortÃ©-Agel, Y.-T. Wu, H. Lu, and R. J. Conzemius. Large-eddy simulation of atmospheric boundary layer flow through wind turbines and wind farms. *Journal of Wind Engineering and Industrial Aerodynamics*, 99(4):154–168, Apr. 2011.

[14] B. Sanderse, S. Pijl, and B. Koren. Review of computational fluid dynamics for wind turbine wake aerodynamics. *Wind Energy*, 14(7):799–819, Oct. 2011.

[15] J. N. Sorensen and W. Z. Shen. Numerical modeling of wind turbine wakes. *Journal of Fluids Engineering*, 124(2):393–399, 2002.

[16] N. Troldborg, J. N. SÃ¸rensen, and R. Mikkelsen. Actuator line simulation of wake of wind turbine operating in turbulent inflow. *Journal of Physics: Conference Series*, 75:012063, July 2007.

[17] S. Wharton and J. K. Lundquist. Assessing atmospheric stability and its impacts on rotordisk wind characteristics at an onshore wind farm. *Wind Energy*, July 2011.

[18] S. Wharton and J. K. Lundquist. Atmospheric stability affects wind turbine power collection. *Environmental Research Letters*, 7(1):014005, Mar. 2012.

[19] Y.-T. Wu and F. PortÃ©-Agel. Large-eddy simulation of wind-turbine wakes: Evaluation of turbine parametrisations. *Boundary-Layer Meteorology*, 138(3):345–366, Dec. 2010.